

Quasioptical modeling of wave beams with and without mode conversion: IV. Numerical simulations of waves in dissipative media

K. Yanagihara,¹ I. Y. Dodin,^{2,3} and S. Kubo⁴

¹*Naka Fusion Institute, National Institutes for Quantum and
Radiological Science and Technology, 311-0193, Naka, Ibaraki, Japan*

²*Princeton Plasma Physics Laboratory, Princeton, New Jersey 08543, USA*

³*Department of Astrophysical Sciences, Princeton University, Princeton, New Jersey 08544, USA*

⁴*National Institute for Fusion Science, National Institutes of Natural Sciences, 509-5292, Toki, Gifu, Japan*

(Dated: November 16, 2021)

We report the first quasioptical simulations of wave beams in a hot plasma using the quasioptical code PARADE (PARaxial RAY DEscription) [Phys. Plasmas **26**, 072112 (2019)]. This code is unique in that it accounts for inhomogeneity of the dissipation-rate across the beam and mode conversion simultaneously. We show that the dissipation-rate inhomogeneity shifts beams relative to their trajectories in cold plasma and that the two electromagnetic modes are coupled via this process, an effect that was ignored in the past. We also propose a simplified approach to accounting for the dissipation-rate inhomogeneity. This approach is computationally inexpensive and simplifies analysis of actual experiments.

I. INTRODUCTION

Modeling of radiofrequency waves in fusion plasmas requires accurate calculations of their power deposition through various resonant mechanisms. For electron-cyclotron (EC) [1, 2] and lower-hybrid [3] waves, which have short enough wavelengths, this is commonly done using geometrical-optics ray tracing [4, 5]. However, this method ignores a number of important effects, including diffraction, so the deposition profiles are often predicted to be more peaked than they are in reality [6]. To deal with this problem, a number of quasioptical models have been proposed [6–17]. However, most of these models [6–13] assume that wave beams maintain a particular (Gaussian) transverse profile, and they also ignore variations of the dissipation-rate within the beam cross section. One exception to this is the model by Balakin *et al.* [14–17]; still, this model assumes single-mode beams and thus cannot describe mode conversion, which is often important [18–20]. To fill the gap, a more comprehensive quasioptical theory and the corresponding code PARADE (PARaxial RAY DEscription) have been developed recently [21–23], and its preliminary applications have already been reported [24].

Here, we report the first applications of PARADE to modeling quasioptical wave beams with mode conversion in hot plasma. Our findings indicate that conventional simulations overlook important effects connected with: (i) the inhomogeneity of the dissipation-rate within the beam cross section and (ii) the O–X mode conversion. The simulations reported here are the first ones that account for these effects simultaneously. We find that the dissipation-rate inhomogeneity shifts wave beams relative to their trajectories in cold plasma. PARADE also predicts that the two plasma modes are coupled via this process, an effect that was ignored in the past. We also propose a simplified approach to accounting for the dissipation-rate inhomogeneity to speed-up the calculations

in a practical fusion plasma geometry.

Our paper is organized as follows. In Sec. II, we briefly overview the theoretical model underlying PARADE. In Sec. III, we introduce the two dissipation models that we use, and we also report the coupling between the X and O modes caused by the dissipation. In Sec. IV, we summarize our main results.

II. THEORETICAL MODEL

A. Basic equations

To describe the theory that underlies PARADE, let us start with the equation for the electric field \mathbf{E} of a linear wave governed by a general dispersion operator $\hat{\mathbf{D}}$:

$$\hat{\mathbf{D}}\mathbf{E} = 0. \quad (1)$$

We assume that the field is stationary, with constant frequency ω , and has an eikonal form $\mathbf{E} = e^{-i\omega t + i\theta(\mathbf{x})}\boldsymbol{\psi}(\mathbf{x})$. (The time dependence is henceforth omitted for brevity.) Here, the scalar function θ is a rapidly varying “reference phase”, $\mathbf{k} \doteq \nabla\theta$ is the local wave vector (the symbol \doteq denotes definitions), and the complex vector $\boldsymbol{\psi}$ is a slowly varying envelope. We also introduce the following small parameters:

$$\epsilon_{\parallel} \doteq \lambda/L_{\parallel}, \quad \epsilon_{\perp} \doteq \lambda/L_{\perp}, \quad \epsilon_{\parallel} \sim \epsilon_{\perp}^2 \ll 1, \quad (2)$$

where $\lambda \doteq 2\pi/k$ is the wavelength, L_{\parallel} is the characteristic scale of the beam field along the group velocity at the beam center, and L_{\perp} is the minimum scale of the field in the plane transverse to the group velocity. The medium-inhomogeneity scale is assumed to be of the same order as L_{\parallel} or larger. Under these assumptions, Eq. (1) can be expressed as

$$\mathbf{D}\boldsymbol{\psi} + \hat{\mathcal{L}}\boldsymbol{\psi} = 0, \quad (3)$$

where the operator $\widehat{\mathcal{L}} = \mathcal{O}(\epsilon_\perp)$ is specified in Ref. [21] (also see below), and the matrix \mathbf{D} is found from the Weyl symbol of $\widehat{\mathbf{D}}$, or the local dispersion matrix \mathbf{D} [21], that satisfies the ordering

$$\mathbf{D}_H = \mathcal{O}(1), \quad \mathbf{D}_A \leq \mathcal{O}(\epsilon_\perp). \quad (4)$$

The indices H and A denote the Hermitian part and the anti-Hermitian part, respectively. For our purposes, it is sufficient to adopt [21]

$$\mathbf{D}_H(\mathbf{x}, \mathbf{p}) = \frac{c^2}{16\pi\omega^2} [\mathbf{p}\mathbf{p} - (\mathbf{p} \cdot \mathbf{p})\mathbb{1}] + \frac{1}{16\pi} \boldsymbol{\varepsilon}_H(\mathbf{x}, \mathbf{p}), \quad (5)$$

$$\mathbf{D}_A(\mathbf{x}, \mathbf{p}) = \frac{1}{16\pi} \boldsymbol{\varepsilon}_A(\mathbf{x}, \mathbf{p}), \quad (6)$$

where $\mathbb{1}$ is a unit matrix and $\boldsymbol{\varepsilon}$ is the dielectric tensor found, for example, in Ref. [25]; its dependence on ω is assumed but not emphasized, since ω is constant. (Here, \mathbf{p} denotes any given wave vector, as opposed to \mathbf{k} , which is the specific wave vector determined by θ ; see above.)

B. Polarization vectors and matrices

Since \mathbf{D}_H is assumed as the dominant part of the dispersion operator in Eq. (3), it is convenient to decompose the envelope $\boldsymbol{\psi}$ in the basis $\{\boldsymbol{\eta}_s\}$ of the orthogonal eigenvectors of \mathbf{D}_H , i.e., $\mathbf{D}_H\boldsymbol{\eta}_s = \Lambda_s\boldsymbol{\eta}_s$. This decomposition can be written as follows:

$$\boldsymbol{\psi} = \boldsymbol{\eta}_o a^o + \boldsymbol{\eta}_x a^x + \bar{\boldsymbol{\eta}} \bar{a}, \quad (7)$$

where a^o , a^x , and \bar{a} are complex coefficients, $\boldsymbol{\eta}_o$ and $\boldsymbol{\eta}_x$ are the polarization vectors of the O- and X-mode in homogeneous plasma, and $\bar{\boldsymbol{\eta}}$ is the third eigenvector of \mathbf{D} that is orthogonal to both of them.

In general, the O and X modes are coupled, which means that both Λ_o and Λ_x are close to zero simultaneously and

$$a^o = \mathcal{O}(1), \quad a^x = \mathcal{O}(1), \quad \bar{a} = \mathcal{O}(\epsilon_\perp). \quad (8)$$

The small amplitude \bar{a} can be calculated perturbatively and does not enter quasioptical equations explicitly. Instead, we work with a two-dimensional amplitude vector

$$\mathbf{a} = \begin{pmatrix} a^o \\ a^x \end{pmatrix} \quad (9)$$

and the 3×2 “polarization matrix” $\boldsymbol{\Xi}$ that contains the vectors $\boldsymbol{\eta}_o$ and $\boldsymbol{\eta}_x$ as its columns,

$$\boldsymbol{\Xi} = \begin{pmatrix} \boldsymbol{\eta}_o & \boldsymbol{\eta}_x \end{pmatrix}. \quad (10)$$

Then, $\boldsymbol{\psi}$ can be expressed as follows:

$$\boldsymbol{\psi} = \boldsymbol{\Xi} \mathbf{a} + \mathcal{O}(\epsilon_\perp). \quad (11)$$

Since we consider the beam dynamics in coordinates that are close to Euclidean, the dual-basis vectors can be

adopted in the form $\boldsymbol{\eta}^o \approx \boldsymbol{\eta}_o$ and $\boldsymbol{\eta}^x \approx \boldsymbol{\eta}_x$, and we also introduce a 2×3 matrix

$$\boldsymbol{\Xi}^+ = \begin{pmatrix} \boldsymbol{\eta}_o^* \\ \boldsymbol{\eta}_x^* \end{pmatrix}. \quad (12)$$

[For more general definitions, see Ref. [21].] As seen easily, this matrix satisfies $\boldsymbol{\Xi}^+ \boldsymbol{\Xi} = \mathbb{1}$, and

$$\boldsymbol{\Lambda} \doteq \boldsymbol{\Xi}^+ \mathbf{D}_H \boldsymbol{\Xi} = \begin{pmatrix} \Lambda_o & 0 \\ 0 & \Lambda_x \end{pmatrix}. \quad (13)$$

In the single-mode case, also considered in Refs. [14–17], the above equations are simplified. For example, assume that a wave consists mainly of the O mode. (The X-mode case is treated similarly.) Then,

$$a^o = \mathcal{O}(1), \quad a^x = \mathcal{O}(\epsilon_\perp), \quad \bar{a} = \mathcal{O}(\epsilon_\perp), \quad (14)$$

and the polarization matrix becomes 3×1 dimensional, $\boldsymbol{\Xi} = \boldsymbol{\eta}_o$, so it is just the O-mode polarization vector. Accordingly,

$$\boldsymbol{\psi} = \boldsymbol{\Xi} a^o + \mathcal{O}(\epsilon_\perp), \quad (15)$$

where the correction $\mathcal{O}(\epsilon_\perp)$ can be found perturbatively but if needed but otherwise is inessential. Similarly, $\boldsymbol{\Xi}^+$ is a row vector in this case, namely, $\boldsymbol{\Xi}^+ = \boldsymbol{\eta}_o^*$. Accordingly, $\boldsymbol{\Xi}^+ \boldsymbol{\Xi} = 1$ and $\Lambda_o \doteq \boldsymbol{\Xi}^+ \mathbf{D}_H \boldsymbol{\Xi}$ is a scalar. This single-mode model is used in simulations reported below in Secs. III A and III B.

C. Reference ray and new coordinates

The evolution of the wave amplitude is considered relative to the a “reference ray” (RR) that is governed by Hamilton’s equations

$$\frac{d\mathbf{X}}{d\zeta} = \frac{1}{V_\star} \frac{\partial H_\star}{\partial \mathbf{K}}, \quad \frac{d\mathbf{K}}{d\zeta} = -\frac{1}{V_\star} \frac{\partial H_\star}{\partial \mathbf{X}}, \quad (16)$$

where \mathbf{X} and \mathbf{K} are the ray coordinate and the ray wavevector, ζ is the path along the ray trajectory, and $V_\star \doteq |\partial H_\star / \partial \mathbf{K}|$ is the absolute value of the group velocity. The ray Hamiltonian H_\star is

$$H_\star \doteq \frac{1}{2} (\Lambda_{\star o} + \Lambda_{\star x}) \quad (17)$$

for a mode-converting beam and $H_\star \doteq \Lambda_{\star s}$ for a single-mode beam. Here and further, the index \star denotes that the corresponding quantity is evaluated on the RR.

Next, we introduce the RR-based curvilinear coordinates $\tilde{x}^\mu \equiv \{\zeta, \tilde{\varrho}^1, \tilde{\varrho}^2\}$, where $\tilde{\varrho}^\sigma$ are, loosely speaking, the orthogonal coordinates on the plane transverse to the group velocity of the RR as specified in [22]. (Here and further, the indices σ and $\bar{\sigma}$ span from 1 to 2; other Greek indices span from 1 to 3.) The basis vectors $\tilde{\mathbf{e}}_\mu$ of the new coordinates ($d\mathbf{x} = \tilde{\mathbf{e}}_\mu d\tilde{x}^\mu$) are defined such that

$$\tilde{\mathbf{e}}_{\star\mu} \cdot \tilde{\mathbf{e}}_{\star\nu} = \delta_{\mu\nu}, \quad \left[\partial \tilde{\mathbf{e}}_\sigma(\tilde{x}) / \partial \tilde{\varrho}^{\bar{\sigma}} \right]_\star = 0. \quad (18)$$

Then,

$$\mathbf{x} \approx \mathbf{X}(\zeta) + (\tilde{\mathbf{e}}_{*1} \ \tilde{\mathbf{e}}_{*2}) \begin{pmatrix} \tilde{\varrho}^1 \\ \tilde{\varrho}^2 \end{pmatrix}. \quad (19)$$

D. Quasioptical equation

To simplify the field equation, we introduce the rescaled complex vector amplitude $\phi = \sqrt{V_*} \mathbf{a}$. Then, as shown in Ref. [23], Eq. (3) leads to the following parabolic equation:

$$\begin{aligned} \frac{\partial \phi}{\partial \zeta} = \frac{1}{V_*} \Big[& -i(\tilde{\mathcal{L}}_{*\sigma\bar{\sigma}} \tilde{\varrho}^\sigma \tilde{\varrho}^{\bar{\sigma}} + \tilde{\mathfrak{M}}_{*\sigma} \tilde{\varrho}^\sigma + \mathbf{M}_* - \mathbf{U}_*) \phi \\ & + \frac{i}{2} \tilde{\Phi}_*^{\sigma\bar{\sigma}} \partial_{\sigma\bar{\sigma}}^2 \phi + \mathbf{\Gamma} \phi \\ & - (\tilde{\mathbf{u}}_*^\sigma + \tilde{\vartheta}_*^{\sigma\bar{\sigma}} \tilde{\varrho}^{\bar{\sigma}}) \partial_\sigma \phi - \frac{\tilde{\vartheta}_*^{\sigma\bar{\sigma}}}{2} \phi \Big], \end{aligned} \quad (20)$$

In the single-mode case, when ϕ is a scalar, one similarly has [22]

$$\begin{aligned} \frac{\partial \phi}{\partial \zeta} = \frac{1}{V_*} \Big[& -i(\tilde{\mathcal{L}}_{*\sigma\bar{\sigma}} \tilde{\varrho}^\sigma \tilde{\varrho}^{\bar{\sigma}} - U_*) \phi + \frac{i}{2} \tilde{\Phi}_*^{\sigma\bar{\sigma}} \partial_{\sigma\bar{\sigma}}^2 \phi \\ & + \Gamma \phi - \tilde{\vartheta}_*^{\sigma\bar{\sigma}} \tilde{\varrho}^{\bar{\sigma}} \partial_\sigma \phi - \frac{\tilde{\vartheta}_*^{\sigma\bar{\sigma}}}{2} \phi \Big], \end{aligned} \quad (21)$$

which is an alternative representation of the field equation assumed in Refs. [14–17]. Here, $\partial_\sigma \doteq \partial/\partial \rho^\sigma$, summation over repeating indices is assumed, and the coefficients are expressed through \mathbf{D} as described in Ref. [23]. Models for $\mathbf{\Gamma}$ are discussed in Sec. III in detail.

III. DISSIPATION IN HOT PLASMA

The matrix $\mathbf{\Gamma}$, which represents dissipation, is given by [23]

$$\mathbf{\Gamma} = \mathbf{\Xi}_*^+ \mathbf{D}_A(\mathbf{x}, \mathbf{k}(\mathbf{x})) \mathbf{\Xi}_*, \quad (22)$$

where \mathbf{D}_A is given by Eq. (6) and $\mathbf{\Xi}_*$ is the polarization matrix [Eq. (10)] evaluated on the RR. (In the single-mode case, $\mathbf{\Xi}_*$ becomes a vector, and then $\mathbf{\Gamma}$ is a scalar.) In an inhomogeneous medium, $\mathbf{\Gamma}$ is inhomogeneous, which results in variation of the dissipation-rate within the beam cross section [Fig. 1(a)]. Most quasioptical codes [6–13] ignore this fact and adopt

$$\mathbf{\Gamma} \approx \mathbf{\Gamma}_* = \mathbf{\Xi}_*^+ \mathbf{D}_{A*} \mathbf{\Xi}_* \quad (23)$$

instead [Fig. 1(b)]. This leads to incorrect predictions for actual heating rates, as discussed in Ref. [26]. In PARADE, we adopt two different models to calculate $\mathbf{\Gamma}$ more accurately, as discussed in Sec. III A and Sec. III B. Also note that unlike in conventional single-mode models that treat the dissipation coefficient as a scalar [6–17, 22], our $\mathbf{\Gamma}$ [Eq. (22)] is generally nondiagonal, so it couples ϕ^o and ϕ^x in Eq. (20). This effect, which we call dissipation-driven mode conversion, is discussed in Sec. III C.

A. Exact dissipation matrix

In one scheme, we calculate $\mathbf{\Gamma}$ at each grid point using Eq. (22) as is [Fig. 1(c)]. Figure 2 illustrates application of this model to a test simulation. Modeled there is the wave-beam propagation in hot-electron plasma with electron density $n = 1.0 \times 10^{19} \text{ m}^{-3}$, electron temperature $T = 2.0 \text{ keV}$, and magnetic field $\{B_x, B_y, B_z\} = \{B \cos \theta, 0, B \sin \theta\}$, with $\theta = 80.0^\circ$,

$$B = B_0 \exp \left[-\left(\frac{x}{L_y} - 1 \right)^2 - \left(\frac{y}{L_y} - 1 \right)^2 \right], \quad (24)$$

$B_0 = 7.3 \text{ T}$, $L_x = 1.5 \text{ m}$, and $L_y = 5.0 \text{ m}$. A single-mode O-wave beam is injected along the x axis from the origin and is initially assumed Gaussian, namely [27],

$$\begin{aligned} a^s = \sqrt{\frac{2}{\pi w_1 w_2}} \exp \Big[& -\frac{(\tilde{\varrho}^1)^2}{w_1^2} - \frac{(\tilde{\varrho}^2)^2}{w_2^2} \\ & + \frac{ik(\tilde{\varrho}^1)^2}{2R_1} + \frac{ik(\tilde{\varrho}^2)^2}{2R_2} + \frac{i}{2}(g_1 + g_2) \Big], \end{aligned} \quad (25)$$

where

$$w_\mu \doteq w_{0,\mu} \sqrt{1 + \varsigma^{-2}}, \quad R_\mu \doteq Z_\mu (1 + \varsigma^2), \quad (26)$$

$$g_\mu \doteq \tan^{-1} \varsigma, \quad \varsigma \doteq k w_{0,\mu} / (2Z_\mu), \quad (27)$$

and $k = 2\pi f/c$, with the focal lengths $Z_1 = Z_2 = 1.5 \text{ m}$, the waist sizes $w_{0,1} = w_{0,2} = 4.0 \text{ cm}$, and the wave frequency is $f = 77.0 \text{ GHz}$, which corresponds to the vacuum wavelength $\lambda_0 \approx 4 \text{ mm}$. The cold-plasma ϵ is used for \mathbf{D}_H , and the hot-plasma ϵ [25] is used for \mathbf{D}_A with six cyclotron harmonics retained. In these settings, O–X conversion is insignificant, so the single-mode version of PARADE [22] was used. Like all simulations reported in this paper, these simulations were done on a laptop with Intel Core™ i7-8569U processor.

Unlike within the homogeneous-dissipation model, the top side of the beam in Fig. 2(b) is strongly distorted by inhomogeneous cyclotron damping. The beam narrows and experiences defocusing due to diffraction, and the location of the beam center

$$\tilde{\varrho}_{\text{center}} \doteq \frac{\int |a^s| \tilde{\varrho} d^2 \tilde{\varrho}}{\int |a^s| d^2 \tilde{\varrho}} \quad (28)$$

shifts down relative to the horizontal line. Note that this shift (marked with black arrows) is unrelated to refraction and cannot be captured by most quasioptical codes. The ability of PARADE to capture such shifts makes it particularly useful for modeling the propagation of wave beams grazing cyclotron resonances. Beams like that are typical in fusion experiments, which involve oblique injection from the mid-plane launcher or arbitrary injection from the top launcher.

Figure 3 shows the total beam power in the same simulation. The homogeneous-dissipation model predicts almost complete absorption of the beam power at the main

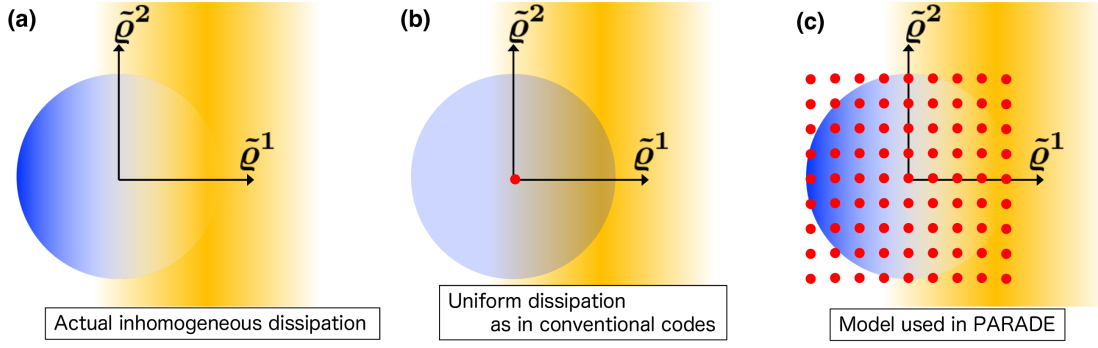


FIG. 1: Schematics of three models of resonant dissipation in an inhomogeneous medium. The wave beam propagates in the direction perpendicular to the figure. The intensity of the blue color denotes the intensity profile in the beam cross section. The intensity of the orange color denotes the local damping rate γ . The red points correspond to the locations at which γ is actually calculated numerically. Figure (a) corresponds to the true inhomogeneous dissipation, in which case the field on the left dissipates more slowly than the field on the right (modulo diffraction). Figure (b) illustrates the homogeneous-dissipation model assumed in most quasioptical codes; in this model, the whole beam dissipates at the rate γ evaluated at the beam center. Figure (c) illustrates the PARADE dissipation model described in Sec. III A.

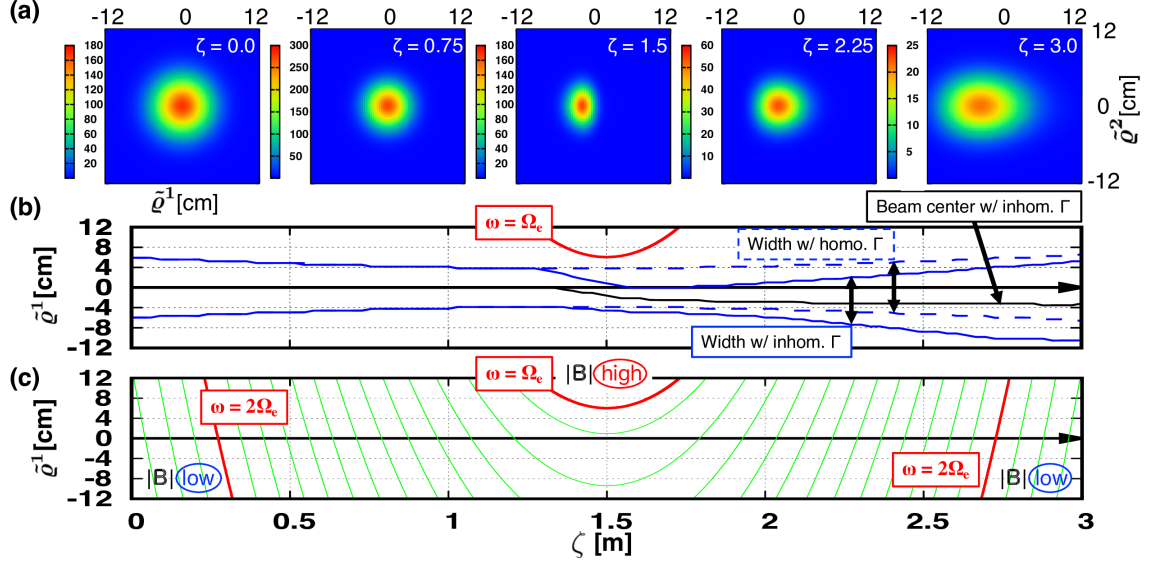


FIG. 2: Results of a test simulation of a wave beam passing near the electron cyclotron resonance within the model described in Sec. III A. Figure (a) shows the transverse cross sections of the beam intensity at $\zeta = 0.75, 1.5, 2.25$, and 3.0 m. Figure (b) shows the evolution of the beam width (blue solid lines) and the trajectory of the beam center (black solid line). The beam width is determined numerically as the distance on which the amplitude $|a|$ drops one e -fold from its maximum along the $\tilde{\rho}^1$ -axis. The beam center is defined as in Eq. (28). As a reference, the blue dashed lines show the corresponding width within the homogeneous-dissipation model [Fig. 1(b)]. Figure (c) shows isosurfaces of the magnetic-field strength [Eq. (24)]. The locations of the first and second electron-cyclotron resonances are marked in red.

cyclotron resonance. In contrast, the inhomogeneous-dissipation model predicts that the beam in fact retains about 20% of its power. This is a significant difference, which is important in experiment [26].

B. Approximate dissipation matrix

Calculating Γ using Eq. (22) is computationally expensive and can be impractical, for example, for data analysis between discharges and for optimization of the launching geometry. Because of this, we also propose a simplified model as an alternative, which is as follows. Assuming that the beam width is smaller than the char-

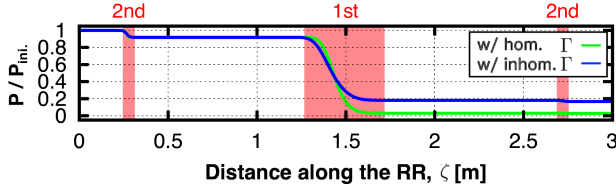


FIG. 3: The total power transported by the same beam as in Fig. 2, in units of the input power. Green: homogeneous-dissipation model as in Fig. 1(b). Blue: inhomogeneous-dissipation model as in Fig. 1(c). The shaded regions denote areas of resonant dissipation at the first (figure center) and second (figure sides) cyclotron harmonics.

acteristic scale of Γ , the latter can be Taylor-expanded to the first order in $\tilde{\varrho}$. To do this, note that

$$\Gamma = \Xi_{\star}^+ D_A(\mathbf{X} + \tilde{\varrho}, \mathbf{K} + \tilde{\pi}(\tilde{\varrho})) \Xi_{\star}, \quad (29)$$

where $\tilde{\pi}(\tilde{\varrho}) \doteq \mathbf{k}(\mathbf{x}) - \mathbf{K}$ can be expressed as [22]

$$\tilde{\pi}_{\mu} = -\frac{1}{V_{\star}^2} \frac{\partial H_{\star}}{\partial \tilde{\varrho}^{\sigma}} \frac{\partial H_{\star}}{\partial \tilde{\pi}_{\mu}} \tilde{\varrho}^{\sigma}. \quad (30)$$

This leads to

$$\Gamma \approx \Gamma_{\star} + \mathcal{G}_{\star\sigma} \tilde{\varrho}^{\sigma}, \quad (31a)$$

$$\mathcal{G}_{\star\sigma} = \frac{\partial \Gamma_{\star}}{\partial \tilde{\varrho}^{\sigma}} - \frac{1}{V_{\star}^2} \frac{\partial H_{\star}}{\partial \tilde{\varrho}^{\sigma}} \frac{\partial H_{\star}}{\partial \tilde{\pi}_{\mu}} \frac{\partial \Gamma_{\star}}{\partial \tilde{\pi}_{\mu}}. \quad (31b)$$

Because the matrix $\mathcal{G}_{\star\sigma}$ has to be calculated only on the RR rather than at each grid point, this approach significantly speeds up calculations. We call it a first-order model. (Accordingly, the homogeneous-dissipation model used in other codes can be classified as the zeroth-model.) For single-mode beams, this approximation is equivalent to that used by Balakin *et al.* [16], but our model extends to mode-converting beams as well. When the first-order term exceeds the zeroth-order term, “numerical pumping” can occur (Fig. 4; see also Ref. [16]). To prevent this spurious effect in practical simulations, we introduce a cutoff:

$$\Gamma_{s's} \approx \begin{cases} \Gamma_{\star s's} + \mathcal{G}_{\star s's\sigma} \tilde{\varrho}^{\sigma}, & \mathcal{G}_{\star s's\sigma} \tilde{\varrho}^{\sigma} \geq -\Gamma_{\star s's}, \\ 0, & \mathcal{G}_{\star s's\sigma} \tilde{\varrho}^{\sigma} < -\Gamma_{\star s's}. \end{cases} \quad (32)$$

Figure 5 demonstrates that the model (32) (blue curves) and the model (22) (orange curves) are in reasonable agreement with test simulations. The simulation using an approximated Γ is eight times faster than the one using the exact Γ (43 s vs. 347 s), and in geometries of practical interest, the speed-up is anticipated to be even larger. However, the simplified model may not be sufficiently accurate when the magnetic-field scales are small enough, as seen in Fig. 5(c).

C. Dissipation-driven mode conversion

The dissipation matrix Γ is generally nondiagonal (Fig. 6), so it couples different components of ϕ in

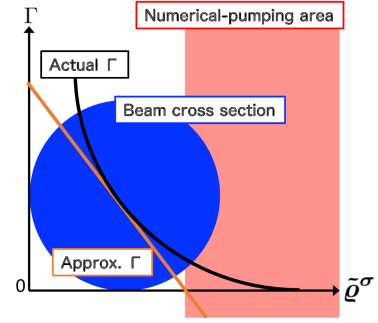


FIG. 4: A schematic of numerical pumping. The blue circle represents the beam cross section. The black curve and the orange line represent the actual dissipation-rate and the approximate dissipation-rate [as in Eq. (31)], respectively. Spurious amplification occurs in the red-shaded area, where the approximate dissipation-rate is negative. A similar discussion can also be found in Ref. [16].

Eq. (20), i.e., causes mode conversion. This is particularly important when the dispersion relations of the two cold-plasma modes differ only slightly, so the coupling is strong. The corresponding applications include multi-pass heating at high harmonics, heating during the ramp-up phase, heating on medium- or small-size fusion devices, and also when off-axis heating is used to eliminate magnetic islands. In these cases, power absorption can be very different from that of a single-mode beam and thus cannot be properly modeled by codes that ignore mode conversion. In contrast, PARADE is naturally suited to handle this problem.

To illustrate the effect of dissipation-driven mode conversion, we have performed a test simulation with the same parameters as in Fig. 6. The initial beam contains O and X modes in equal proportions and is Gaussian in shape [Eq. (25)], with $Z_1 = Z_2 = 2.0$ m and $w_{0,1} = w_{0,2} = 5.0$ cm. Figure 7 (a) shows the fraction of the remaining wave power, $1 - P_{\text{tot}}/P_{\text{ini}}$. Also, Figs. 7 (b): $(P_{x,\text{ini}} - P_x)/P_{\text{ini}}$ and (c): $(P_{o,\text{ini}} - P_o)/P_{\text{ini}}$ show the remaining X- and O-components, respectively. Here $P_{\text{ini}} = P_{x,\text{ini}} + P_{o,\text{ini}}$ is the total input power, $P_{\text{tot}} = P_x + P_o$ is total absorbed power, and P_x and P_o are defined as follows:

$$\begin{pmatrix} P_x \\ P_o \end{pmatrix} \doteq \begin{pmatrix} P_{xx} + P_{xo} \\ P_{ox} + P_{oo} \end{pmatrix}, \quad (33a)$$

$$P_{s's} = \int a^{s'} \Gamma_{s's} a^s d^2 \tilde{\varrho}. \quad (33b)$$

The orange curves in each Figs. 7 (a)-(c) represent simulations where the dissipation-driven mode conversion is taken into account. For a reference, the blue curves represent simulations where mode conversion (i.e., the terms P_{xo} and P_{ox}) is ignored.

The impact of the mode coupling on the total power absorption is significant, as seen from the deviation of the orange curve from the blue curve in Fig. 7 (a). Notably,

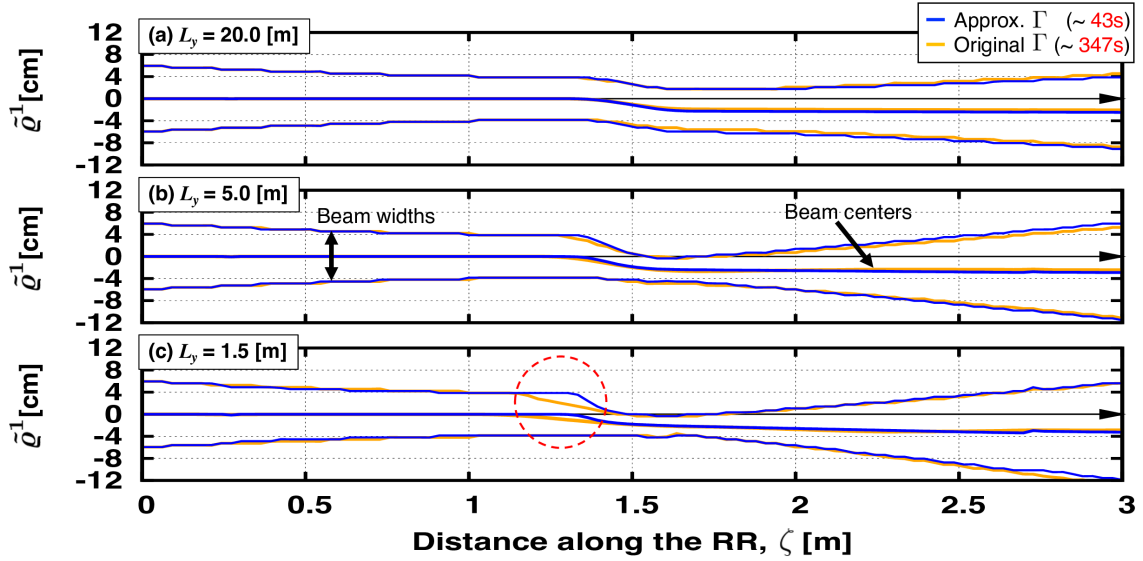


FIG. 5: Test-simulation results showing a comparison of the two models for Γ used in PARADE. The curves illustrate the evolution of the beam widths and the beam center. Blue: approximate model (31). Orange: original model (22). The simulation setup is the same as in Fig. 2, except three different values are used for the magnetic-field scale: (a) $L_y = 20$ m, (b) $L_y = 5$ m, and (c) $L_y = 1.5$ m. The discrepancy between the two dissipation models is more pronounced at the smallest L_y , as marked with a red circle in figure (c). The calculation using the approximate model is eight times faster.

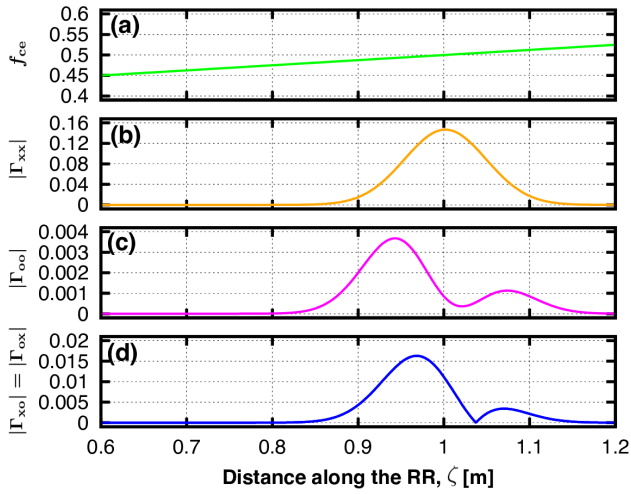


FIG. 6: Plasma parameters along the RR trajectory in a test simulation. Figure (a) shows the electron cyclotron frequency f_{ce} in units $f = 140.0$ GHz, which corresponds to the vacuum wavelength $\lambda_0 \approx 2$ mm. Figures (b)–(d) show the individual elements of Γ . Here, the density is $n = 1.0 \times 10^{19} \text{ m}^{-3}$, the temperature is $T = 10$ keV, the magnetic field is $\{B_x, B_y, B_z\} = \{B \cos \theta, 0, B \sin \theta\}$, with $\theta = 85.0^\circ$ and $B = B_0(x + x_0)/L_x$, where $B_0 = 2.5$ T, $x_0 = 3.0$ m, and $L_x = 4.0$ m. The wave is injected along the x axis from the origin.

as seen from Fig. 7 (b) and (c), while X mode components with sufficiently high dissipation-rate are completely dissipated for both simulations, O mode component with

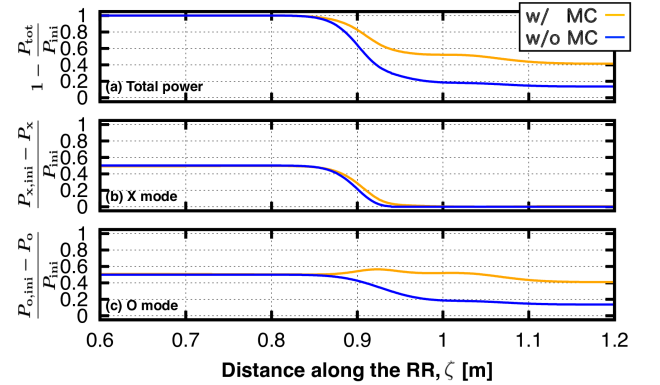


FIG. 7: The fractions of the remaining wave power in the same simulation as in Fig. 6. (a), (b), and (c) correspond to the result for total power: $1 - P_{\text{tot}}/P_{\text{ini}}$, X mode component: $(P_{x,\text{ini}} - P_x)/P_{\text{ini}}$, and O mode component: $(P_{o,\text{ini}} - P_o)/P_{\text{ini}}$, respectively. Here, $P_{\text{tot}} \doteq P_x + P_o$ is the total absorbed power [Eq. (33)], and $P_{\text{ini}} \doteq P_{x,\text{ini}} + P_{o,\text{ini}}$ is the total input power. The orange curves represent simulations where the dissipation-driven mode conversion is taken into account. For a reference, the blue curves represent simulations where mode conversion is ignored. A significant difference is appeared between both approach, especially for the O mode component P_o , as seen from (c).

mode conversion is increased unlike those without mode conversion. Also note that although the polarization state of the wave was chosen here arbitrarily, calculating it for a practical experiment may also require PARADE

simulations, such as those described in Ref. [23].

IV. CONCLUSIONS

Here, we report the first quasioptical simulations of wave beams in a hot plasma using the quasioptical code PARADE (PARaxial RAY DEscription). This code [21–23] is unique in that it accounts for inhomogeneity of the dissipation rate across the beam and mode conversion simultaneously. We show that the dissipation-rate inhomogeneity shifts beams relative to their trajectories in cold plasma and that the two electromagnetic modes are coupled via this process, an effect that was ignored in the past. We also propose a simplified approach to

accounting for the dissipation-rate inhomogeneity. This approach is computationally inexpensive and simplifies analysis of actual experiments. Our results lay the foundation for comparing PARADE simulations with experimental data, as to be reported in our next paper [26].

V. ACKNOWLEDGMENTS

The work was supported by the U.S. DOE through Contract No. DE-AC02-09CH11466. The work was also supported by JSPS KAKENHI Grant Number JP17H03514.

-
- [1] M. Bornatici, R. Cano, O. D. Barbieri, and F. Engelmann, *Electron cyclotron emission and absorption in fusion plasmas*, Nucl. Fusion **23**, 1153 (1983).
 - [2] V. Erckmann and U. Gasparino, *Electron cyclotron resonance heating and current drive in toroidal fusion plasmas*, Plasma Phys. Control. Fusion **36**, 1869 (1994).
 - [3] P. T. Bonoli, *Linear theory of lower hybrid heating*, in IEEE Transactions on Plasma Science **12**, 95 (1984).
 - [4] I. B. Bernstein, *Geometric optics in space- and time-varying plasmas*, Phys. Fluids **18**, 320 (1975).
 - [5] L. Friedland and I. B. Bernstein, *Geometric optics in plasmas characterized by non-Hermitian dielectric tensors*, Phys. Rev. A **22**, 1680 (1980).
 - [6] E. Poli, A. G. Peeters, and G. V. Pereverzev, *TORBEAM, a beam tracing code for electron-cyclotron waves in tokamak plasmas*, Comput. Phys. Commun. **136**, 90 (2001).
 - [7] E. Poli, G. V. Pereverzev, A. G. Peeters, and M. Bornatici, *EC beam tracing in fusion plasmas*, Fusion Eng. Des. **53**, 9 (2001).
 - [8] E. Poli, A. Bock, M. Lochbrunner, O. Maj, M. Reich, A. Snicker, A. Stegmeir, F. Volpe, N. Bertelli, R. Bilato, G. D. Conway, D. Farina, F. Felici, L. Figini, R. Fischer, C. Galperti, T. Happel, Y. R. Lin-Liu, N. B. Marushchenko, U. Mszanowski, F. M. Poli, J. Stober, E. Westerhof, R. Zille, A. G. Peeters, and G. V. Pereverzev, *TORBEAM 2.0, a paraxial beam tracing code for electron-cyclotron beams in fusion plasmas for extended physics applications*, Comput. Phys. Commun. **225**, 36 (2018).
 - [9] G. V. Pereverzev, *Beam tracing in inhomogeneous anisotropic plasmas*, Phys. Plasmas **5**, 3529 (1998).
 - [10] E. Mazzucato, *Propagation of a Gaussian beam in a non-homogeneous plasma*, Phys. Fluids B **1**, 1855 (1989).
 - [11] S. Nowak and A. Orefice, *Quasioptical treatment of electromagnetic Gaussian beams in inhomogeneous and anisotropic plasmas*, Phys. Fluids B **5**, 1945 (1993).
 - [12] A. G. Peeters, *Extension of the ray equations of geometric optics to include diffraction effects*, Phys. Plasmas **3**, 4386 (1996).
 - [13] D. Farina, *A quasi-optical beam-tracing code for electron cyclotron absorption and current drive: GRAY*, Fusion Sci. Tech. **52**, 154 (2007).
 - [14] A. A. Balakin, M. A. Balakina, G. V. Permitin, and A. I. Smirnov, *Quasi-optical description of wave beams in smoothly inhomogeneous anisotropic media*, J. Phys. D: Appl. Phys. **40**, 4285 (2007).
 - [15] A. A. Balakin, M. A. Balakina, G. V. Permitin, and A. I. Smirnov, *Scalar equation for wave beams in a magnetized plasma*, Plasma Phys. Rep. **33**, 302 (2007).
 - [16] A. A. Balakin, M. A. Balakina, G. V. Permitin, and A. I. Smirnov, *Effect of dissipation on the propagation of wave beams in inhomogeneous anisotropic and gyrotropic media*, Plasma Phys. Rep. **34**, 486 (2008).
 - [17] A. A. Balakin, M. A. Balakina, and E. Westerhof, *ECRH power deposition from a quasi-optical point of view*, Nucl. Fusion **48**, 065003 (2008).
 - [18] I. Y. Dodin, D. E. Ruiz, and S. Kubo, *Mode conversion in cold low-density plasma with a sheared magnetic field*, Phys. Plasmas **24**, 122116 (2017).
 - [19] T. I. Tsujimura, S. Kubo, H. Takahashi, R. Makino, R. Seki, Y. Yoshimura, H. Igami, T. Shimoizuma, K. Ida, C. Suzuki, M. Emoto, M. Yokoyama, T. Kobayashi, C. Moon, K. Nagaoka, M. Osakabe, S. Kobayashi, S. Ito, Y. Mizuno, K. Okada, A. Ejiri, T. Mutoh, and the LHD Experiment Group, *Development and application of a ray-tracing code integrating with 3D equilibrium mapping in LHD ECH experiments*, Nucl. Fusion **55**, 123019 (2015).
 - [20] S. Kubo, H. Igami, T. I. Tsujimura, T. Shimoizuma, H. Takahashi, Y. Yoshimura, M. Nishiura, R. Makino, and T. Mutoh, *Plasma interface of the EC waves to the LHD peripheral region*, AIP Conf. Proc. **1689**, 090006 (2015).
 - [21] I. Y. Dodin, D. E. Ruiz, K. Yanagihara, Y. Zhou, and S. Kubo, *Quasioptical modeling of wave beams with and without mode conversion: I. Basic theory*, Phys. Plasmas **26**, 072110 (2019).
 - [22] K. Yanagihara, I. Y. Dodin, and S. Kubo, *Quasioptical modeling of wave beams with and without mode conversion: II. Numerical simulations of single-mode beams*, Phys. Plasmas **26**, 072111 (2019).
 - [23] K. Yanagihara, I. Y. Dodin, and S. Kubo, *Quasioptical modeling of wave beams with and without mode conversion: III. Numerical simulations of mode-converting beams*, Phys. Plasmas **26**, 072112 (2019).

- [24] K. Yanagihara, S. Kubo, T. I. Tsujimura, and I. Y. Dodin, *Mode purity of electron cyclotron waves after their passage through the peripheral plasma in the Large Helical Device*, Plasma Fusion Res. **14**, 3403103 (2019).
- [25] T. H. Stix, *Waves in Plasmas* (AIP, New York, 1992).
- [26] K. Yanagihara, S. Kubo, and I. Y. Dodin and the LHD experiment Group, *Quasioptical propagation and absorption of electron cyclotron waves: simulation and experiment*, in preparation.
- [27] A. Yariv, *Quantum Electronics* (Wiley, New Jersey, 1967).